Hindawi
International Journal of Optics
Volume 2020, Article ID 1695658, 15 pages
https://doi.org/10.1155/2020/1695658

Research Article

Multispectral Polarization State Analyzer of Scanning Polarimeter ScanPol

Ivan Syniavskyi,[1] **Yevgen Oberemok**,[2] **Yuriy Ivanov**,[1] **and Mikhail Sosonkin**[1]

[1]*Main Astronomical Observatory National Academy of Science of Ukraine, Kyiv, Ukraine*
[2]*Taras Shevchenko National University of Kyiv, Kyiv, Ukraine*

Correspondence should be addressed to Ivan Syniavskyi; syniavskyi@gmail.com

Received 11 May 2020; Revised 17 July 2020; Accepted 17 August 2020; Published 26 October 2020

Academic Editor: Chenggen Quan

We present the results of the development of a representational model of the multispectral polarization state analyzer of the ScanPol scanning polarimeter for the space experiment Aerosol-UA. The aim of the Ukrainian space mission Aerosol-UA is to create a database based on continuous satellite measurements of the optical characteristics of aerosol and cloud particles in the Earth's atmosphere over a long period of time. The ScanPol polarimeter is designed to acquire spatial, temporal, and spectral-polarimetric measurements simultaneously to minimize instrumental "parasitic" effects and effects of "false" polarizations due to scene movement. Simultaneity is provided by separation of the initial spatial field by a pair of conjugated telescopes and a pair of Wollaston prisms. ScanPol provides to measure the first three Stokes parameters I, Q, and U of the radiation reflected by atmospheric aerosols and the Earth's surface for a six solar reflectance spectral bands in the near ultraviolet (NUV), visible (VIS), and near-infrared (NIR) spectral channels centered in the wavelengths 370 nm, 410 nm, 555 nm, 865 nm, 1378 nm, and 1620 nm. Stokes parameters I, Q, and U are used to determine a degree of linear polarization of radiation that will allow obtaining the phase function and polarization characteristics of aerosol particle scattering, estimate their size, and determine the aerosol type and optical thickness. The polarimeter optical layout is considered, and the spectral characteristics of the transmission of optical channels are given. Obtained signal-to-noise ratio exceeded 500 for wavelengths 370 nm and 410 nm and exceeded 1000 for other wavelengths. The design of the chosen photodetectors is based on surface mount type photodiodes: Si-photodiodes Hamamatsu S10356-01 for the optical range of 370–860 nm and InGaAs-photodiodes Hamamatsu G8941-011620 for wavelengths 1378 nm and 1620 nm. The effect of orientation of Wollaston prisms axes on polarization measurement error is considered. The errors of azimuth mount of Wollaston prisms ≤2 arcmin in ScanPol leads to error of degree of linear polarization ≤0.0012.

1. Introduction

The impact of aerosol particles in the Earth's atmosphere on climate by many estimates can be compared to the magnitude of the greenhouse gases effect.

To date, there are several space missions to study the distribution of aerosols in the Earth's atmosphere, for example, MISR/terra, OMI/aura, AVHHR, MODIS/terra/aqua, CALIOP/CALIPSO, and GOME-2 [1–3]. In order to improve the quality of data for climate models and reduce the uncertainty of calculations of radiative forcing, a number of new space experiments are planned to study aerosols.

After a successful long-term operation of the POLDER/PARASOL CNES aerosol mission, the improved aerosol polarimeter for the 3MI/EPS-SG project is scheduled to be launched in 2020 or later. There are also other missions/tools, namely, the NASA MAIA mission carries the Multiangle SpectroPolarimetric Imager (MSPI) [4], the NASA PACE mission carries the SPEXone tool [5], and the HARP-2 tool. The direction polarimetric camera (DPC) operates on-board the Chinese GaoFen-5 satellite recently launched by the Chinese Space Agency [6].

The Ukrainian space mission Aerosol-UA [7] is prepared with main objective to monitor the microphysics and spatial distribution of atmospheric aerosols. The mission includes

the multispectral Scanning Polarimeter (ScanPol) and the MultiSpectral Imaging Polarimeter (MSIP), which is planned to launch in 2022. The ScanPol polarimeter is designed on principles of the APS/glory polarimeter [8]. It has six solar reflectance spectral bands in the near ultraviolet (NUV), visible (VIS), and near-infrared (NIR) spectral channels centered in the wavelengths 370 nm, 410 nm, 555 nm, 865 nm, 1378 nm, and 1620 nm that measure the first three Stokes parameters I, Q, and U of the radiation reflected by atmospheric aerosols and the Earth's surface at about 200 viewing directions in between scanning angles +50° and −60° degrees from nadir. The polarimeter is designed to acquire spatial, temporal, and spectral-polarimetric measurements simultaneously to minimize instrumental "parasitic" effects and effects of "false" polarizations due to scene movement. Simultaneity is provided by separation of the initial spatial field by a pair of conjugated telescopes and a pair of Wollaston prisms. One telescope provides simultaneous measurements intensities of the linear polarization components in orthogonal planes at 0° and 90° to the meridional plane of the instrument, while the other telescope simultaneously measures equivalent intensities in orthogonal planes at 45° and 135°.

In this paper, we present the results of the development of the polarization state analyzer (PSA) of the ScanPol polarimeter. The design of the optical system and the description of the spectral selection system are given. We also present the preliminary estimation of the signal-to-noise ratio and theoretical estimation of the error of the azimuth of the Wollaston prism assembly to achieve the given accuracy.

2. Purpose and Composition of the Polarization State Analyzer

2.1. Determination of Stokes Parameters. The aerosol is a sufficiently variable atmospheric component that is characterized by a large number of parameters, such as particle size, quantity, shape, internal structure, their absorption, scattering properties, and their spatial distribution. As a result of the uncertainties of all these parameters in climate models, the impact of aerosol on climate and environment are considered to be one of the most uncertain factors.

Multiangle polarimetry is one of the most promising tools of remote sensing for a detailed study of atmospheric aerosols. In [9, 10], the possibility of multispectral multiangle photo-polarimetric satellite remote sensing to perform a simultaneous retrieval of aerosol and cloud properties for partly cloudy scenes and for fully cloudy scenes where the aerosol layer is located above the cloud was shown. The last requires polarimetric measurement accuracy <0.002 and radiometric accuracy <4%. The multispectral PSA of the ScanPol considered in this paper is designed to meet these requirements.

Photo-polarimetric observations are conducted over a wide range of scattering angles; they cover a wide spectral range and provide significant additional information on aerosol characteristics.

Solar radiation is scattered by the presence of aerosols in the Earth's atmosphere, and it can be partially polarized. The nature and degree of polarization depend on the scattering conditions and scattering parameters. The relationship between the scattering observation conditions, the scattering parameters, and the scattering polarization is used to investigate aerosols.

The light polarization is described by four Stokes parameters [11]. Parameter I describes the total light intensity, and the other three parameters (Q, U, and V) describe its polarization. These parameters can be obtained by determining the six intensities:

$$\begin{pmatrix} I \\ Q \\ U \\ V \end{pmatrix} = \begin{pmatrix} I_0 + I_{90} \\ I_0 - I_{90} \\ I_{45} - I_{-45} \\ I_r - I_l \end{pmatrix}, \tag{1}$$

where I_0, I_{90}, I_{45}, I_{-45}, I_r, and I_l are, respectively, the light intensities with vertical and horizontal polarizations, polarizations with angles 45° and −45°, and right- and left-circular polarizations, which are measured directly by the photometric method. The intensities I_0, I_{90}, I_{45}, and I_{-45} can be measured by linearly polarizing elements, while I_r and I_l can be obtained by using a quarter-wave plate and a linear polarizer.

The angle of inclination of the large axis of the polarization ellipse with respect to the X axis (azimuth of polarization) is defined as

$$\psi = \frac{1}{2}\operatorname{arctg}\left(\frac{U}{Q}\right). \tag{2}$$

The degree of linear polarization is defined as

$$P_{\text{lin}} = \frac{\sqrt{Q^2 + U^2}}{I}. \tag{3}$$

The degree of circular polarization is defined as

$$P_{\text{cir}} = \frac{V}{I}. \tag{4}$$

The total degree of polarization is defined as

$$P = \frac{\sqrt{Q^2 + U^2 + V^2}}{I}. \tag{5}$$

The value of the Stokes parameter V, which characterizes the circular component of light polarization, is always less than the value of the other three Stokes parameters (by at least two orders of magnitude) [12]. Therefore, the majority of polarimeters of the corresponding space missions are aimed at measuring exactly the first three Stokes parameters of the scattered solar light [13].

Thus, to determine the parameters I, Q, and U, it is sufficient to have measurements of the intensities of light in two pairs of mutually orthogonal polarization directions rotated relative to each other by an angle of 45°.

2.2. Optical Layout. The PSA of the ScanPol is designed to analyze the polarization of the light scattered by the Earth's

surface and the atmosphere in the spectral range of 370–1620 nm. It is divided into six bands. This separation is explained by the purpose of the spectral channels: the channel of 370 nm is designed to evaluate the absorption capacity of the troposphere aerosol and its vertical distribution; the channel of 410 nm is intended for the aerosol analysis over the ocean and the Earth's surface; the channel of 555 nm is used to determine the ocean color and aerosol analysis; the channel of 865 nm is required for the aerosol analysis over the ocean and land; the channel of 1378 nm is for the separation of cirrus clouds and stratospheric aerosols and for the separation of tropospheric and stratospheric aerosols in the case of volcanic eruptions; the channel of 1620 nm is to assess the contribution of the surface of the measured signal over the land.

With the aim to simplify the optical layout and to maintain the required signal-to-noise ratio, the spectral selection system is divided into the VIS and IR parts. The VIS part selects bands 370 nm, 410 nm, and 555 nm from the incoming light using three pairs of dichroic mirrors and three pairs of UV interference filters. The IR part is structurally identical to the VIS one and selects near-infrared bands of 865 nm, 1378 nm, and 1620 nm.

To measure the Stokes parameters I, Q, and U in the specified spectral bands, each of the parts (VIS and IR) contains two units VIS-1, VIS-2 and IR-1, IR-2, respectively (Figure 1). The units VIS-1 and IR-1 contain Wollaston prisms with 0° azimuths, at the output of which the o (ordinary) and e (extraordinary) rays have intensities of I_0 and I_{90}, respectively. The units VIS-2 and IR-2 contain Wollaston prisms with azimuths of 45°, at the output of which o and e beams have intensities of I_{45} and I_{-45}, respectively.

The optical layout of the ScanPol instrument is shown in Figure 1. It is based on the concept of the NASA glory space mission, which aimed to monitor the spatial and temporal distributions of the main characteristics of tropospheric and stratospheric aerosols in the Earth's atmosphere using an APS polarimeter [8]. Each of the ScanPol optical blocks consists of

(1) Entrance telescope system, which forms an intermediate image of the observed object; field diaphragm; collimator

(2) A Wollaston prism that splits light into components I_0 and I_{90} (I_{45}, I_{-45}) with orthogonal polarization, and thus, it functions as a polarization analyzer in accordance with equation (3).

(3) Dichroic mirrors and spectral filters, which define a narrow spectral range $\Delta\lambda$ per band

(4) Camera lenses, which form two pairs of images I_0, I_{90} and I_{45}, I_{-45} on detectors

Figure 1 shows that the Wollaston prisms in the units are input before the spectral selection elements since their polarization characteristics can be considered identical in the indicated spectral bands.

The optical layout of the VIS channel of the ScanPol instrument is shown in Figure 2.

The main parameters of the PSA are presented in Table 1. Table 2 shows information about the number of photo detectors and their type depending on the spectral range. Table 3 shows requirements to ScanPol's PSA.

2.3. Spectral Selection System. The spectral selection system of the units VIS-1, VIS-2, IR-, and IR-2 consists of a dichroic mirror and a spectral filter for each of the six spectral channels. The parameters of the transmission/reflection system and the dichroic mirror-spectral filter were optimized in such a way to have the maximum transmission coefficients in the spectral channels. By the light propagation direction in optical units,

(1) For the spectral channel of 370 nm, the light is selected by a dichroic mirror 340–380 and a spectral filter

(2) For the spectral channel of 410 nm, the light is selected by a dichroic mirror 340–380, which, for the spectral range (410 nm, $\Delta\lambda = 20$ nm), transmits radiation by a dichroic mirror 390–430 and by a spectral filter

(3) For the 555 nm spectral channel, the light is selected by the dichroic mirrors 340–380 and 390–430, which, for the spectral range (555 nm, $\Delta\lambda = 20$ nm), transmit radiation by a spectral filter

The spectral characteristics of the individual dichroic mirrors and spectral filters and the resulting characteristics for spectral channels 370 nm, 410 nm, and 555 nm of the optical units VIS are shown in Figure 3.

By the light propagation direction in optical units IR-1 and IR-2:

(1) For the spectral channel of 865 nm, the light is selected by a dichroic mirror 800–900 and a spectral filter

(2) For the spectral channel of 1378 nm, the light is selected by a dichroic mirror 800–900, which, for the spectral range (1378 nm, $\Delta\lambda = 40$ nm), transmits radiation by a dichroic mirror 1010–1500 and by a spectral filter

(3) For the 1620 nm spectral channel, the light is selected by the dichroic mirrors 800–900 and 1010–1500, which, for the spectral range (1620 nm, $\Delta\lambda = 40$ nm), transmits radiation by a spectral filter.

It should be noted that the residual transmittance of the spectral channel filters of 1378 nm and 1620 nm is outside of the main band in the visible spectrum and is used for the visual positioning of the infrared photodetectors. In whatever follows, it will not affect the measurement results, since it is beyond the IR detector spectral sensitivity.

The spectral characteristics of the individual dichroic mirrors and spectral filters and the resulting characteristics for spectral channels 865 nm, 1378 nm, and 1620 nm of the optical units IR are shown in Figure 4. Note that the individual spectral transmittance values of the VIS and IR optical units will be taken into account in the calibration procedure described in detail in [14].

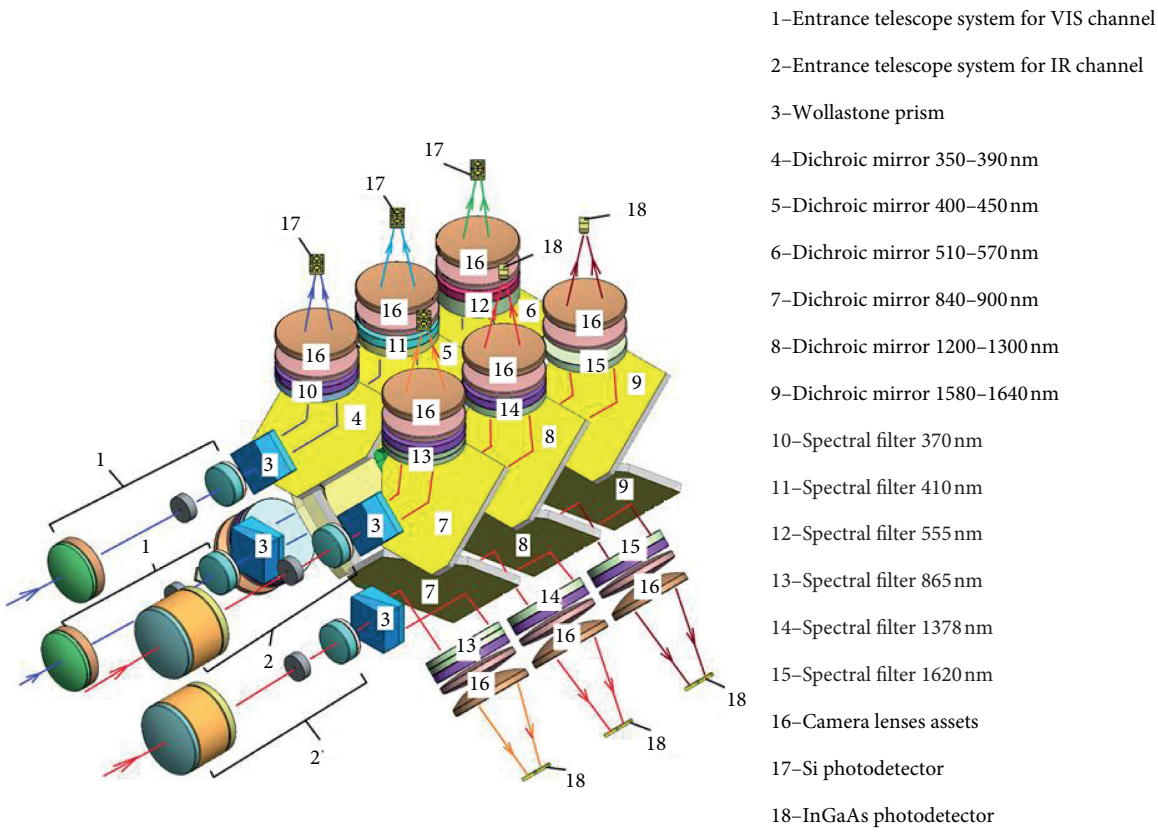

Figure 1: ScanPol polarimeter optical layout.

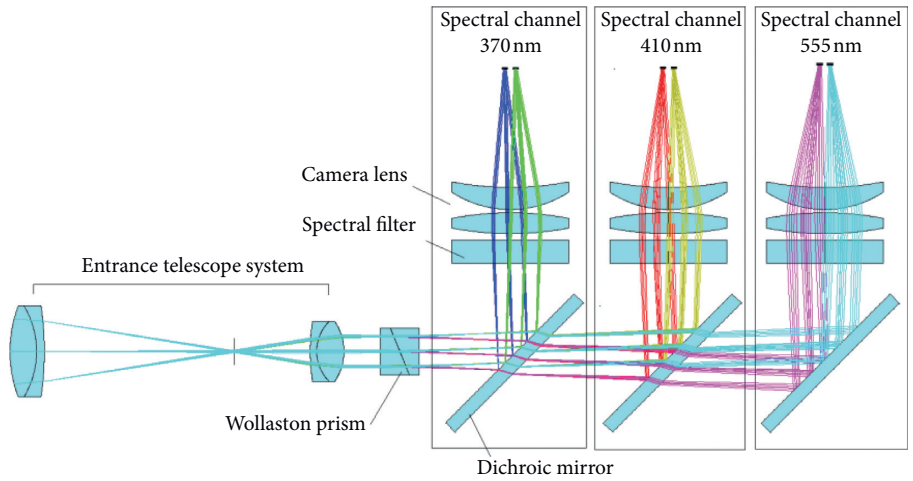

Figure 2: The optical layout of the VIS channel of the ScanPol instrument.

2.4. Detectors of Optical Channel VIS and IR. The choice of photodetectors is determined by the spectral sensitivity and noise characteristics. Another factor in this choice is the design features of the device optical layout.

As noted above, it is necessary to obtain four values of intensities I_0, I_{90}, I_{45}, and I_{-45} to determine the first three Stokes parameters. This is provided by the use of two Wollaston polarization prisms in each of the VIS-1, VIS-2, IR-1, and IR-2 blocks. In fact, in the focal plane of the camera lens, we have two images (i.e., scattering spots) of the field diaphragm for each spectral range. The total number of camera lenses is 12. For example, Figures 5 and 6 show the theoretical scattering spots of the I_0, I_{90}, and (I_{45}, I_{-45}) light components for the spectral channels 555 nm and 1620 nm. The linear size of the scattering spots is up to 0.6 mm for all spectral ranges.

A comparative analysis of the design and dimensions of the optical system has been previously performed to

Table 1: Main parameters of the ScanPol's PSA optical system.

Parameter	Optical unit VIS	Optical unit IR
FOV (°)	0.5	
Enter lens diameter (mm)	10.0	15.0
Enter lens focal length (mm)	32.0	32.0
Collimator diameter (mm)	9.2	9.2
Collimator focal length (mm)	14.9	15.2
Camera lens diameter (mm)	19.5	19.5
Camera lens focal length (mm)	22.0	22.4
Spectral channel quantity	3	3
Wavelength (full width at half maximum), nm	370 (10) 410 (20) 555 (20)	865 (40) 1378 (40) 1620 (40)
Wollaston prism		
Size (mm)	10 × 10	
Separation angle, °	10°	

Table 2: ScanPol photodetectors.

Photodetector substance	Spectral sensitivity (nm)	Quantity
Si	360–900	16
InGaAs	800–1700	8

Table 3: Main requirements to ScanPol's PSA.

Parameter	Value
Azimuth of polarization error -$\Delta\psi$	≤0.2°
Degree of linear polarization error P_{lin}	≤0.15
Photometric error -ΔI	≤4%
SNR	>500
Wollaston prism alignment error $\Delta\varepsilon$	≤3 arcmin
Divergence value of optical axis of the input telescope system	≤6 arcsec

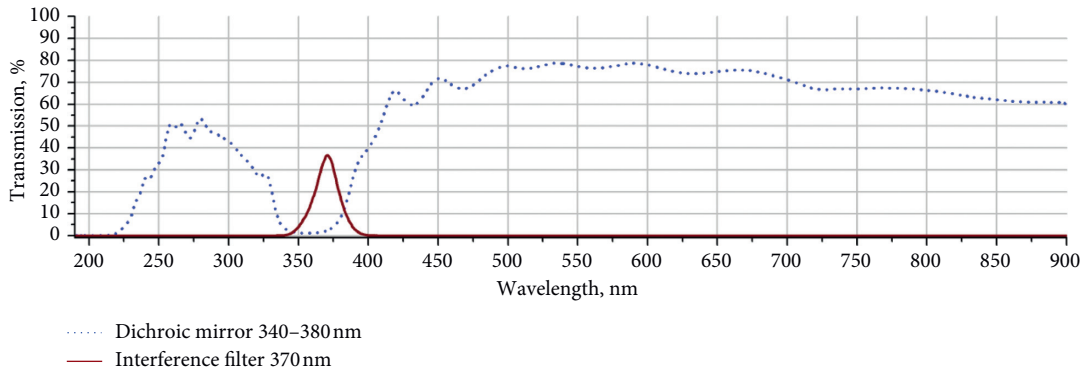

(a)

Figure 3: Continued.

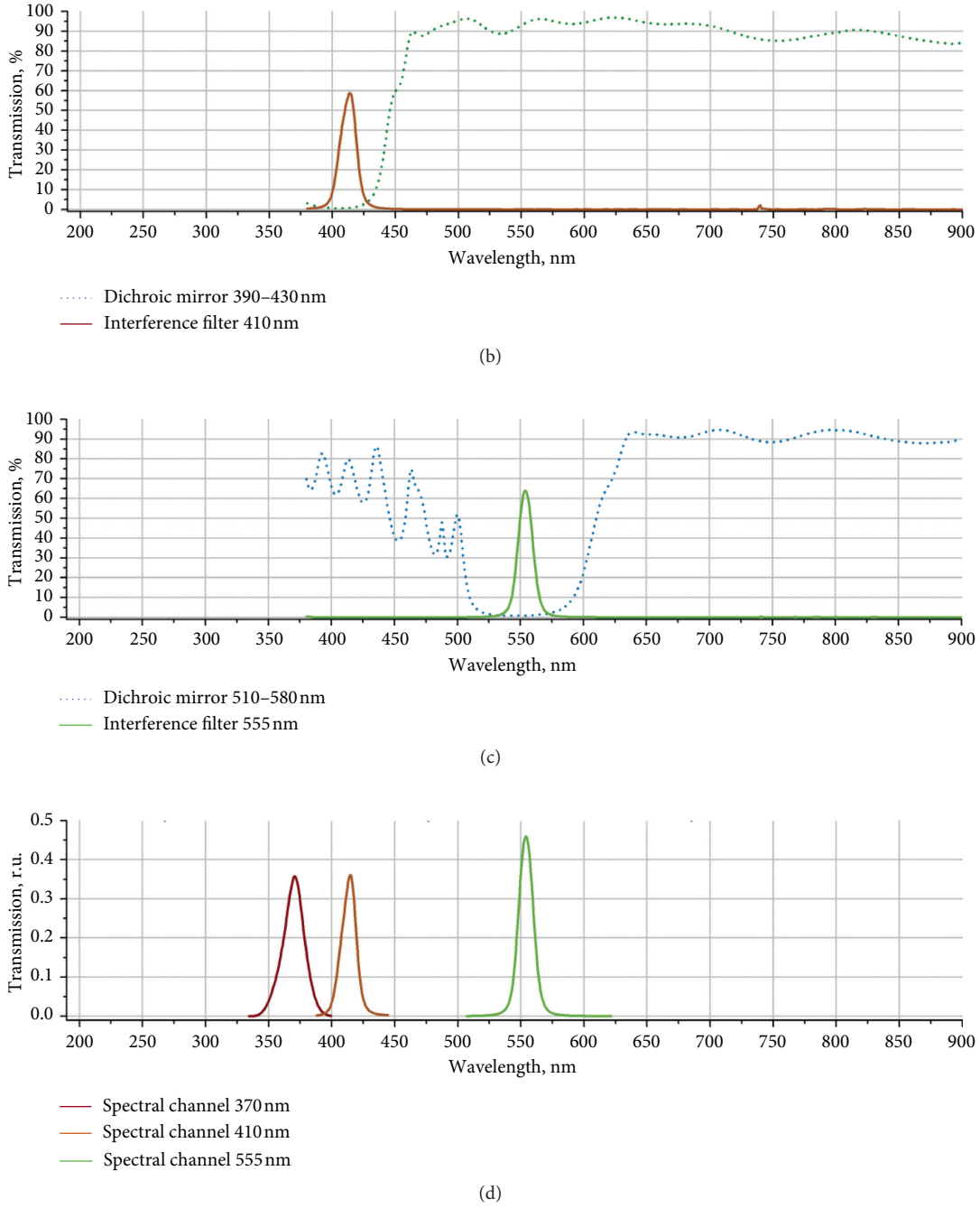

FIGURE 3: Characteristics of the individual dichroic mirrors and spectral filters and the resulting characteristics for spectral channels 370 nm, 410 nm, and 555 nm of the optical units VIS.

determine the optimal configuration of the scattering spots and their spatial diversity in the focal plane of each of the camera lenses. This gives the requirements for the geometric parameters of the photodetectors of each spectral channel that are schematically presented in Figure 7.

The design of the chosen photodetectors for the spectral channels in the optical range of 370–1620 nm is based on surface mount type photodetectors using Si photodiodes-S10356-01 (Hamamatsu) and InGaAs photodiodes-G8941-01 (Hamamatsu). The implementation of each pair of photodiodes is shown in Figure 8.

2.5. Preliminary ScanPol Signal/Noise Ratio Estimate. The signal-to-noise ratio estimate is based on ENVISAT satellite experimental data (IUP-IFE, University of Bremen) [15]. These data are spectral density of the energy brightness of the Earth's surface $B(\lambda)$. They differ in accuracy, in how they

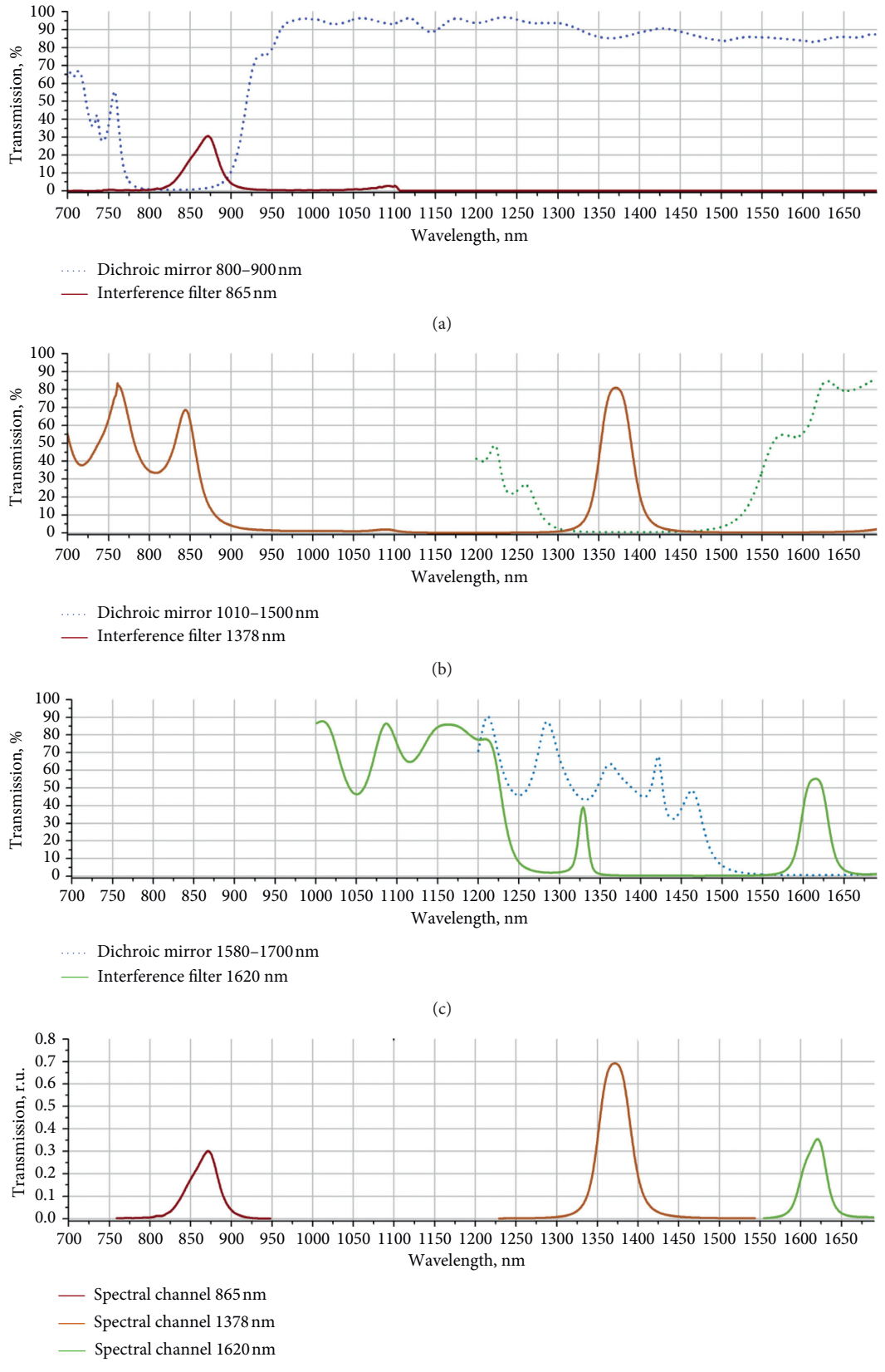

Figure 4: Characteristics of the individual dichroic mirrors and spectral filters and the resulting characteristics for spectral channels 865 nm, 1378 nm, and 1620 nm of the optical units IR.

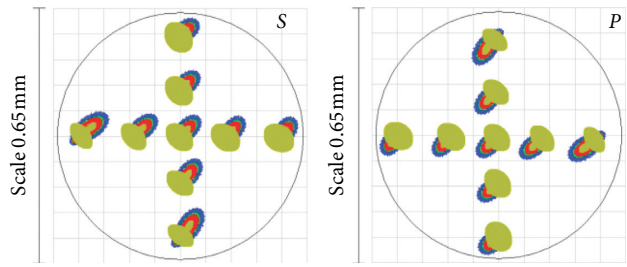

Figure 5: Theoretical spot diagram. The 555 nm spectral channel for (*o*) (*S*) and (*e*) (*P*) light components.

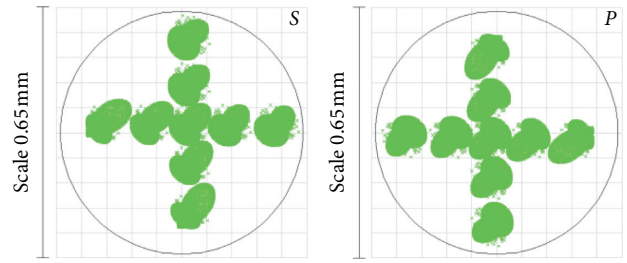

Figure 6: Theoretical spot diagram. The 1620 nm spectral channel for (*o*) (*S*) and (*e*) (*P*) light components.

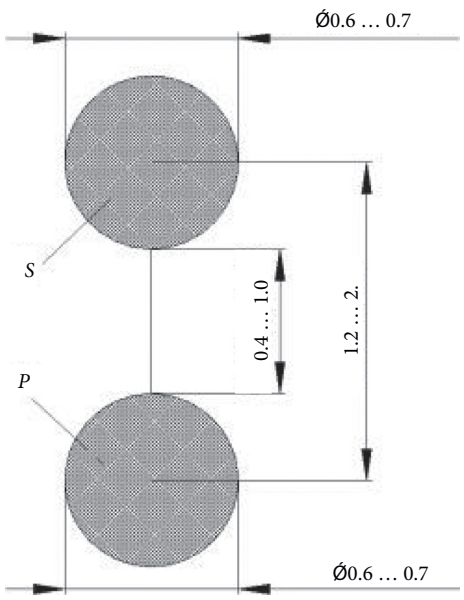

Figure 7: Geometrical parameters of the two-element photodetector to detect the (*o*) (*S*) and (*e*) (*P*) light component.

account for the atmosphere and in their format. If the brightness B of the object and the geometric factor G of the space experiment are known, then the light energy F at the photodetector will be determined by

$$F = \mathrm{BG}. \tag{6}$$

For each channel, the integral energy brightness B_f is calculated as the integral of $B(\lambda)$ within the band of each spectral filter, taking into account the transmission curve

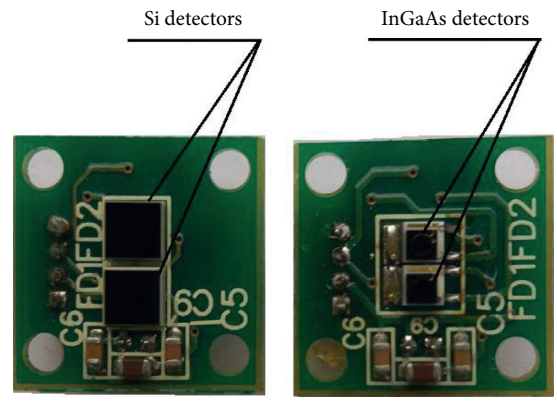

Figure 8: Design solutions of photodetectors for the optical units VIS and IR.

and the transmission/reflection curves of the dichroic mirrors. The geometric factor of the experiment is equal to

$$G = \frac{S\pi D^2}{4H^2}, \tag{7}$$

where $S = 21.53 \times 10^6\, m^2$ is the area of the view on the Earth's surface in nadir; $D = 0.01$ m and 0.015 m are diameters of the entrance lenses of the VIS and IR units; $H = 7 \times 10^5$ m is the height of the satellite orbit.

The electron flux from the photodetector will be equal to

$$n = B_f G \tau \eta t, \tag{8}$$

where B_f is the energy brightness within the spectral band of the channel; G is the geometric factor of the optical system; $\tau = 0.37$ is the average transmittance in the spectral channels (including Wollaston prism); η is the photodetector quantum efficiency; and $t = 1.2 \times 10^{-3}$ sec is the exposure time.

Table 4 shows the input data and the results of the signal to-noise ratio estimate.

3. Assembly and Alignment

3.1. Procedure of Entrance Lenses Mounting and Alignment of View of Field. The main requirement for the design of PSA ScanPol is to combine the field of view of the four input telescopic systems. The alignment requirement is less than 3 arcmin (0.1 magnitude of the field of view). The alignment of the optical axes of the input lenses takes several steps. In step 1 (Figure 9), the field of view of each of the incoming lenses is aligned with the barrel outer diameter. The assembled input lens is mounted in the frame. We fix the position of the field aperture using a microscope and a camera. We rotate the input lens around its own axis and minimize the field aperture displacement using the adjusting screws. In this way, we align the optical axis of the input lens with the axis of the barrel outer diameter. These operations are performed with each of the four input lenses.

In step 2 (Figure 9, right), the input telescopes are alternately mounted in the frame. When installing the first telescope VIS-1, we control the position of the image of a point source of light, and by aligning the unit, we bring it to

Table 4: The signal/noise ratio estimate.

Spectral channel (nm)	370	410	555	865	1378	1620
Geometrical factor G, m^2·steradian	4.70^{-99}			12.0^{-99}		
Energy brightness (scene averaged) B_f photons/sec m^2·steradian,·10^{16}	93.00	70.95	111.27	261.92	35.46	117.61
Photodetector quantum efficiency, η	0.20	0.31	0.72	0.24	0.68	0.51
The number of electrons from the photodetector, n	33.9×10^4	45.9×10^4	168×10^4	335×10^4	128×10^4	319×10^4
Fractional noise, e	582	677	1296	1830	1131	1786
Signal/noise ratio	546	646	1280	1785	1058	1741

The last row of the table shows the signal-to-noise ratio based on the expected noise of the photodetectors, amplifiers, and ADCs.

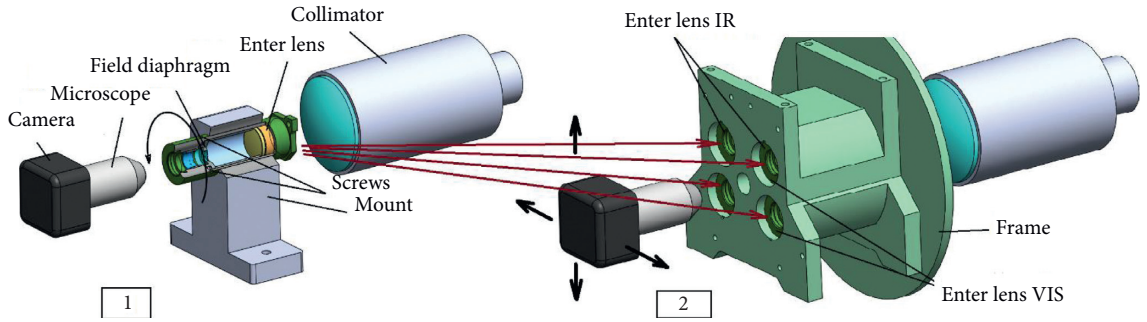

Figure 9: The bench of alignment of field of view of ScanPol PSA entrance lenses.

the center of the field aperture and consider this channel as a reference. We fix the position of the unit. Subsequently, we set up the input telescopes VIS-2, IR-1, and IR-2 and control the position of image of the point source in each channel. If the displacement from the center is within tolerance, the alignment of the view of the input lenses of the telescopic systems is complete. Subsequently, a collimator is installed in the mechanical body of each telescopic system.

Figure 10 schematically shows the results obtained when determining the axis difference of the input telescopic systems VIS-1, VIS-2, IR-1, and IR-2. As described above, the VIS-1 channel (reference channel) was adopted at the start of the reference, and Table 5 presents the values of the differences of the sight axes of the input telescopic systems of the optical units VIS and IR.

3.2. Mount of Wollaston Prisms and Requirements to Their Relative Orientation. To measure the Stokes parameters I, Q, and U of the scattered sunlight, PSA ScanPol contains four Wollaston polarizing prisms, two per VIS and IR units, respectively. To directly determine the Stokes parameters I, Q, and U according to (1), the polarization axes of the prisms in the unit should be oriented at angles $\theta_{W1} = 0^\circ$ and $\theta_{W2} = 45^\circ$ (Figure 11), in the ScanPol coordinate system (XYZ).

We estimate the effect of the error ε in the mounting of the azimuths of the prism axes in the ScanPol units in the XOY plane with respect to the exact values on the error in finding the azimuth (2) and the degree of the linear polarization of light. Given the identity of the structure of VIS and IR ScanPol units, the following estimate is valid for both units.

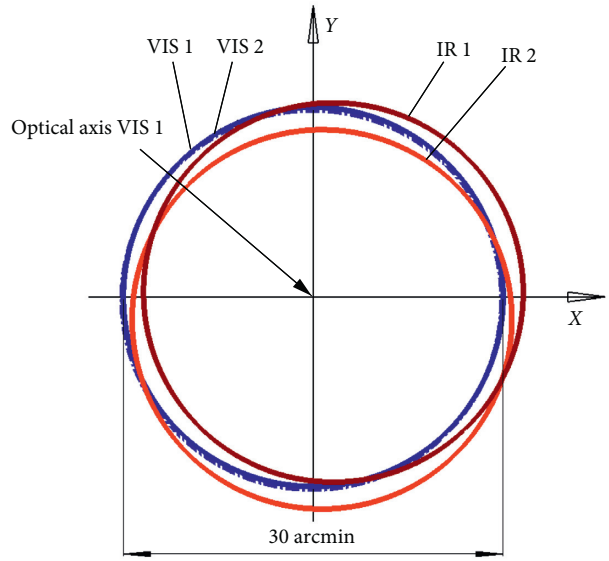

Figure 10: Position of optical axis input telescope VIS-1, 2 and IR-1, 2.

Table 5: Divergence value of optical axis of the input telescope system VIS-1, 2 and IR-1, 2.

Telescopic system	Residual divergence
VIS-1	Reference channel
VIS-2	2 arcmin
IR-1	1 5 arcmin
IR-2	1 5 arcmin

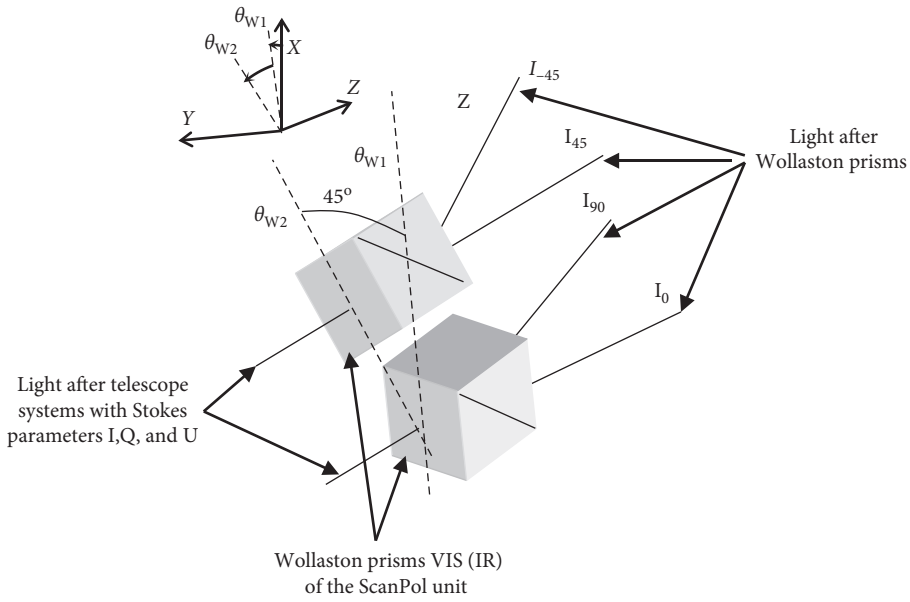

Figure 11: Orientation of the polarizing axes of Wollaston prisms in the ScanPol coordinate system.

The light intensity at the output of the linear polarizer I_θ with the azimuth of the transmission axis θ is related to the Stokes I, Q, U, and V parameters of the input light as

$$I_\theta = \frac{1}{2}\left(I + Q\cos(2\theta) + U\sin(2\theta)\right). \tag{9}$$

At this stage, we have not considered the following: the probable difference in the transmission coefficients of the different optical paths of ScanPol, the finite polarization contrast (extinction ratio) of polarizing prisms, the possible optical anisotropy of the camera lenses, and the other imperfections in the optical characteristics of the PSA ScanPol, which can also significantly affect the field parameters. [14, 16–18]. Because the mount and determination of the orientation of the polarizing axes of the Wollaston prisms are the simplest operations in the PSA ScanPol, it makes sense to investigate separately their effect on the accuracy of measuring the polarization parameters of the light flux.

To determine the first three Stokes light flux parameters, it is sufficient to measure the intensities only at three different orientations θ (6) of the linear polarizer in front of the polarimeter photodetector. Choosing the specific values of these azimuths affects the error in determining the Stokes parameters. The optimal difference between the azimuths is 60°. In this case, the condition number of the instrumental matrix of the polarimeter is at the minimum, which, in turn, minimizes the measurement error of the Stokes parameters [19]. The analysis of the ScanPol polarimeter instrumental matrix, which works in accordance with (1), showed that its scheme is also optimal in terms of minimizing the error in Stokes parameter measurements.

Assuming the uniformity of the ray parameters at the input of two Wollaston prisms with azimuths 0° and 45°, the intensity of the four rays at the output can be estimated from (9) by substituting the values 0°, 90°, 45°, and −45° for θ, respectively:

$$\begin{aligned} I_0 &= \frac{1}{2}(I + Q), \\ I_{90} &= \frac{1}{2}(I - Q), \\ I_{45} &= \frac{1}{2}(I + U), \\ I_{-45} &= \frac{1}{2}(I - U). \end{aligned} \tag{10}$$

Equation (10) shows that the first three Stokes parameters can be calculated from equation (1).

The deviation of the prism azimuths axes from the positions $\theta_{W1} = 0°$ and $\theta_{W2} = 45°$ to the angles ε_1 and ε_2, respectively, will change (10) to the following forms:

$$\begin{aligned} I_{0+\varepsilon_1} &= \frac{1}{2}\left(I + Q\cos(2\varepsilon_1) + U\sin(2\varepsilon_1)\right), \\ I_{90+\varepsilon_1} &= \frac{1}{2}\left(I - Q\cos(2\varepsilon_1)\right) - U\sin(2\varepsilon_1), \\ I_{45+\varepsilon_2} &= \frac{1}{2}\left(I - Q\sin(2\varepsilon_2) + U\cos(2\varepsilon_2)\right), \\ I_{-45+\varepsilon_2} &= \frac{1}{2}\left(I + Q\sin(2\varepsilon_2) - U\cos(2\varepsilon_2)\right). \end{aligned} \tag{11}$$

Using (1) to calculate the Stokes parameters, we obtain

$$
\begin{aligned}
I' &= I = I_{0+\varepsilon_1} + I_{90+\varepsilon_1} = I_{45+\varepsilon_2} + I_{-45+\varepsilon_2},\\
Q' &= I_{0+\varepsilon_1} - I_{90+\varepsilon_1} = Q\cos(2\varepsilon_1) + U\sin(2\varepsilon_1)\\
&= Q - 2\sin(\varepsilon_1)(Q\sin(\varepsilon_1) - U\cos(\varepsilon_1)),\\
U' &= I_{45+\varepsilon_2} - I_{-45+\varepsilon_2} = -Q\sin(2\varepsilon_2) + U\cos(2\varepsilon_2)\\
&= U - 2\sin(\varepsilon_2)(U\sin(\varepsilon_2) + Q\cos(\varepsilon_2)),
\end{aligned}
\tag{12}
$$

where I, Q, and U are the real values of the Stokes light parameters, and Q' and U' are the values of the Stokes parameters with an error. As can be seen from (12), $I = I'$ is a consequence of the high accuracy of the orthogonality of the polarization vectors of the beam pairs (o and e) at the output of each Wollaston prism.

From (12), it can be seen that the systematic errors in determining the Stokes parameters ΔQ and ΔU caused by the inaccurate determination of the polarizing axes of the Wollaston prisms are, respectively,

$$
\begin{aligned}
\Delta Q &= -2\sin(\varepsilon_1)Q\sin(\varepsilon_1) - U\cos(\varepsilon_1),\\
\Delta U &= -2\sin(\varepsilon_2)(U\sin(\varepsilon_2) + Q\cos(\varepsilon_2)).
\end{aligned}
\tag{13}
$$

To estimate the degree P'_{lin} and the angle ψ' of linear polarization of light, we obtain

$$
P'_{\text{lin}} = \frac{\sqrt{Q'^2 + U'^2}}{I} = \sqrt{P_{\text{lin}}^2 + \Delta P^2},
\tag{14}
$$

where

$$
\Delta P^2 = \frac{\left(2(\Delta Q Q + \Delta U U) + \Delta Q^2 + \Delta U^2\right)}{I^2},
\tag{15}
$$

$$
\psi' = \frac{1}{2}\operatorname{arctg}\left(\frac{U'}{Q'}\right).
\tag{16}
$$

The errors of azimuth mounts of Wollaston prisms are $|\varepsilon_{1,2}| \le 2$ arcmin in ScanPol. Using (9)–(16), we obtain that the error of determining the degree of linear polarization is

$$
\Delta P_{\text{lin}} \le 0.0012, \quad \text{when required, } \Delta P_{\text{lin}} \le 0.0015,
\tag{17}
$$

and the error in determining the azimuth of linear polarization is

$$
\Delta\psi \le 2\text{arcmin},
\tag{18}
$$

where $P_{\text{lin}} = |P'_{\text{lin}} - P_{\text{lin}}|$, $\Delta\psi = |\psi' - \psi|$.

We note that estimate (18) is valid only for $\Delta P_{\text{lin}} \neq 0$ because for $\Delta P_{\text{lin}} \neq 0$, the concept of azimuth of linear polarization is meaningless.

Thus, the error in establishing the azimuths of the Wollaston prisms in ScanPol-$|\varepsilon_{1,2}| \le 2$ arcmin is formally acceptable to provide the claimed required accuracy of determining the degree of light polarization ($\Delta P_{\text{lin}} = 0.0015$ at the output of chamber lenses 1 and 2 (Figure 1) by means of (3) without additional calibrations. However, due to other error sources, calibration is likely to be needed. Thereby, condition $\Delta P_{\text{lin}} = 0.0015$ must be considered rather as principal reachable error minimum by $|\varepsilon_{1,2}| \le 2$ arcmin, but in the worst case of maximum, $P_{\text{lin}} \sim 1$ (Figure 12).

In the case where the deviations $|\varepsilon_{1,2}| > 2$ arcmin and their values are known with an error of $|\varepsilon_{1,2}| \le 2$ arcmin, the estimates (17) and (18) will also be valid if the degree and azimuth of linear polarization are found in the standard way by (2) and (3). The Stokes parameters, however, should be determined from (12) as

$$
\begin{pmatrix} Q \\ U \end{pmatrix} = \begin{pmatrix} \cos(2\varepsilon_1) & \sin(2\varepsilon_1) \\ -\sin(2\varepsilon_2) & \cos(2\varepsilon_2) \end{pmatrix}^{-1} \begin{pmatrix} Q' \\ U' \end{pmatrix}.
\tag{19}
$$

Figure 13 shows the maximum dependency values max P_{lin} and max $(\Delta\psi)$ with respect to the error $\Delta\varepsilon = |\Delta\varepsilon_1| + |\Delta\varepsilon_2|/2$ in the worst case when $\Delta\varepsilon_1 = \Delta\varepsilon_2$.

Figure 13 shows that the maximum values of max (P_{lin}) and max $(\Delta\psi)$ are linearly dependent on $\Delta\varepsilon$.

In (17), (18), and Figure 13, the upper estimates are given, whereas from (13), it is clear that the local values of P_{lin} and $\Delta\psi$, except ε_1 and ε_2, depend also on the current values of P_{lin} and ψ of the input light (Figure 12 and [16]).

The minimums of the error ΔP_{lin} in Figure 12(a) correspond to the values of the azimuth $\psi = 0^\circ + \varepsilon_1, 45^\circ + \varepsilon_2, 90^\circ + \varepsilon_1$, and $135^\circ\varepsilon_2$ This is because, for the specified azimuths of the polarization of the input light, first, the intensity of the rays at the output of one of the Wollaston prisms is aligned (respectively, the value of one of the Stokes vectors approaches 0), second, the intensity of one of the beams at the output of the second prism approaches zero, and third, the intensity of the second beam approaches the maximum value of $\text{IP}_{\text{lin}} \gg \Delta Q(\Delta U)$, which determines the minimum error of ΔP_{lin}.

The minimum of error-$\Delta\psi$ in Figure 12(b) corresponds to the values of the azimuth $\psi = 22.5^\circ + \varepsilon_1 - \varepsilon_1/2 + n45^\circ$ (where n is an arbitrary natural number) for which $Q = U \approx 0.7(I \cdot P_{\text{lin}})$ comprising 70% of the maximum possible value. Therefore, $Q, U \gg \Delta Q(\Delta U)$, and their relation is minimally different from the relation Q', V'.

The orientation of the polarization axes of the Wollaston prisms in the VIS and IR channels of PSA ScanPol was performed with accuracy 2 arcmin using a premounted reference Glan prism. The absolute error of P_{lin} is sensitive to the relative orientation of the Wollaston prisms, but insensitive to an external coordinate system rotation. In contrast, the absolute orientation of the Wollaston prisms impacts the absolute error of ψ, and therefore, it must be determined each time the Stokes analyzer block is mounted to PSA. Below, we assumed that indetermination in absolute orientation of Wollaston prisms is smaller than 2 arcmin.

In Figure 14, a general view of the optical mechanical unit ScanPol is presented.

4. Analysis of the Field Aperture Images in the Focal Plane of the Camera Lens

The ghosts from optical surfaces were analyzed. The main sources of highest intensity are the surfaces closest to the focal plane of the camera lens. First of all, it is the surface of spectral filters and dichroic mirrors. In particular, to

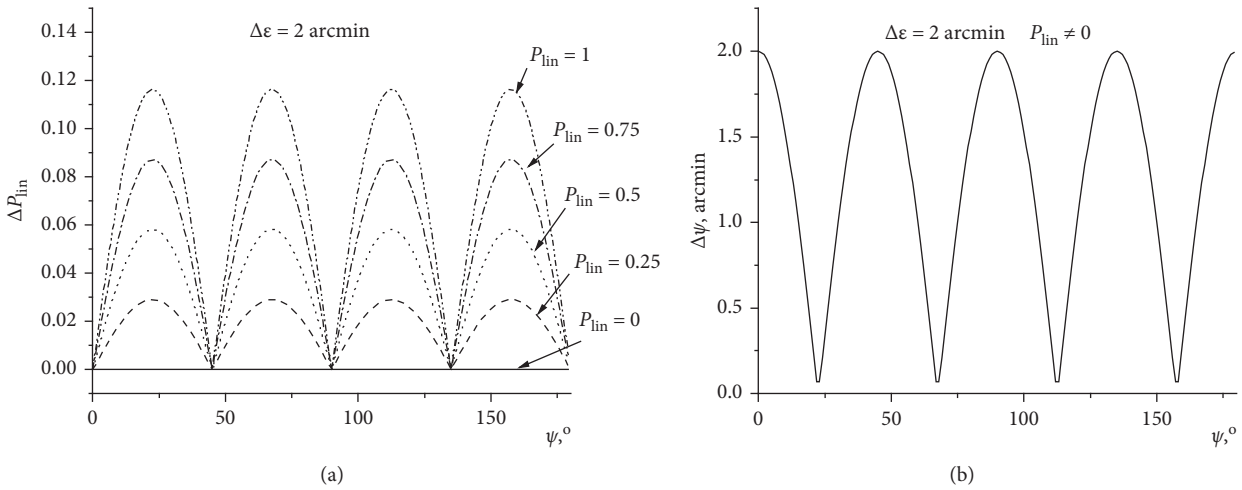

Figure 12: Dependence of the errors ΔP_{lin} and azimuth $\Delta\psi$ of linear polarization of the light on the azimuth of polarization ψ at different values of the degree of P_{lin}, polarization, with the error $\Delta\varepsilon = 2$ arcmin of mount azimuths of the Wollaston prisms.

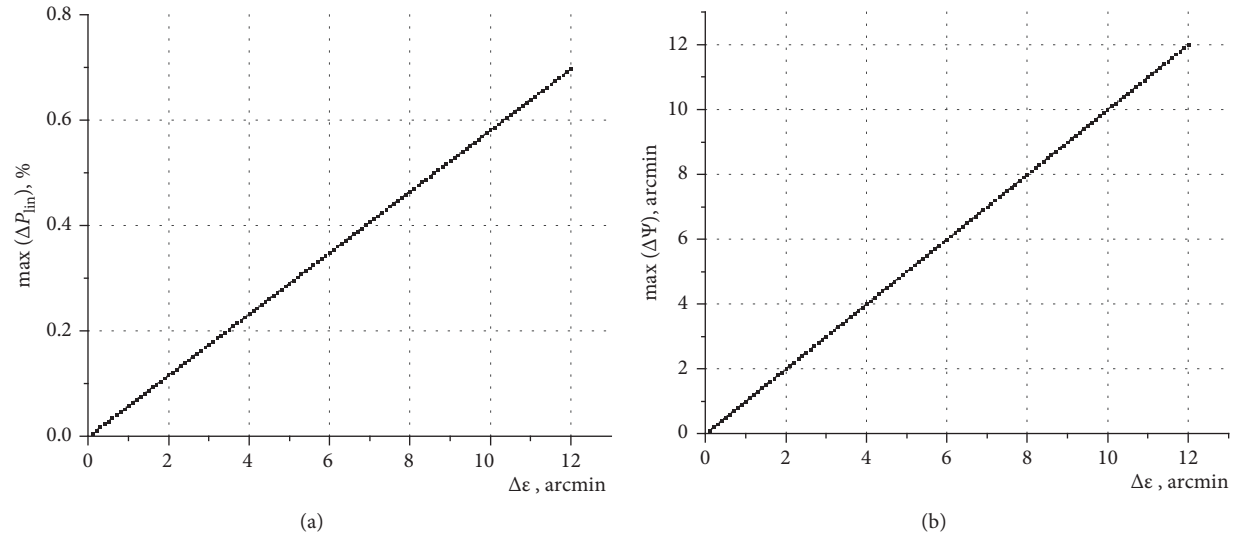

Figure 13: Dependence of the maximum error of determination of the degree of linear polarization P_{lin} (a) and the maximum error of definition of the azimuth of linear polarization $\Delta\psi$ on the error $\Delta\varepsilon = |\Delta\varepsilon_1| + |\Delta\varepsilon_2|/2$ at $\Delta\varepsilon_1 = \Delta\varepsilon_2$ (b).

Figure 14: General view of the PSA ScanPol.

minimize their effect, an antireflection coating is applied to every second surface of the dichroic mirror at the appropriate wavelength.

The ghosts from the optical surfaces of the elements of the spectral selection were experimentally determined in each of the spectral channels and blocked by additional field diaphragms mounted directly near the surface of the photodetectors. Residual stray light level reduction after implementation of the diaphragms amounted to less than 3% for all spectral channels.

The bench, which is used for the noted operations, is shown in Figure 15. It includes the source of light (halogen lamp with a condenser), the PSA ScanPol, the microlens which project the diaphragm images on the CMOS detector, and the computer (laptop).

In Figures 16 and 17, the images of field diaphragms (diameters 0.8–0.9 mm) of the PSA ScanPol's entrance

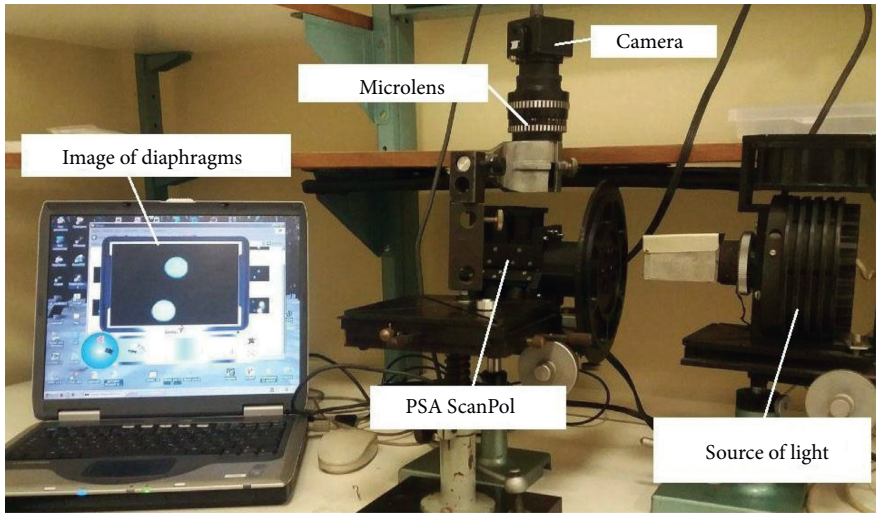

Figure 15: Bench for installation and alignment of PSA unit detectors.

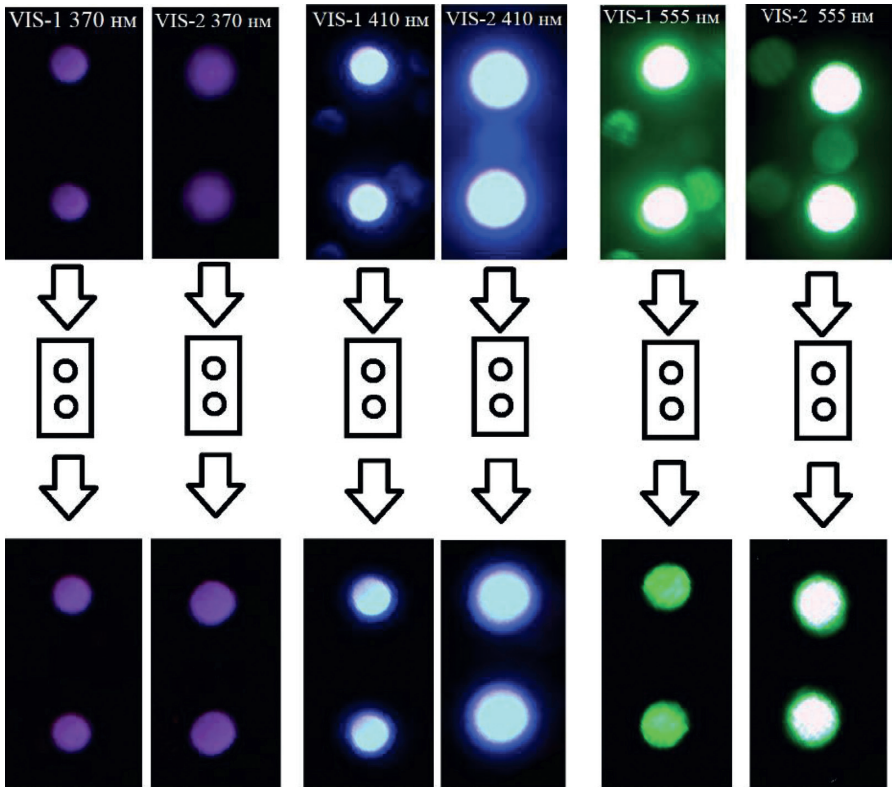

Figure 16: Image of field diaphragm in the focal planes of camera lenses for VIS-1 and VIS-2 units before and after input of blocking diaphragms.

telescope system for each ScanPol spectral channel before and after the introduction of additional cutting apertures are presented.

Although a simplified polarization model of the ScanPol optical channels is used in this paper, it allows us to estimate the fundamentally minimum achievable error in the degree of polarization and azimuth of polarization of the incoming light in ScanPol, given the accuracy of determining the orientation of the Wollaston prism axes.

A complete polarization model of the ScanPol is described in [14]. In particular, it takes into account the individual transmittance values of the ScanPol optical paths, the individual spectral sensitivities of the photodetectors, the noise characteristics of the photodetectors, the individual optical anisotropy of the camera lenses, the finite individual value of the polarization contrast of the Wollaston prisms, and the partial depolarization of light by scattering in optical elements. In [14], a complex procedure of polarization

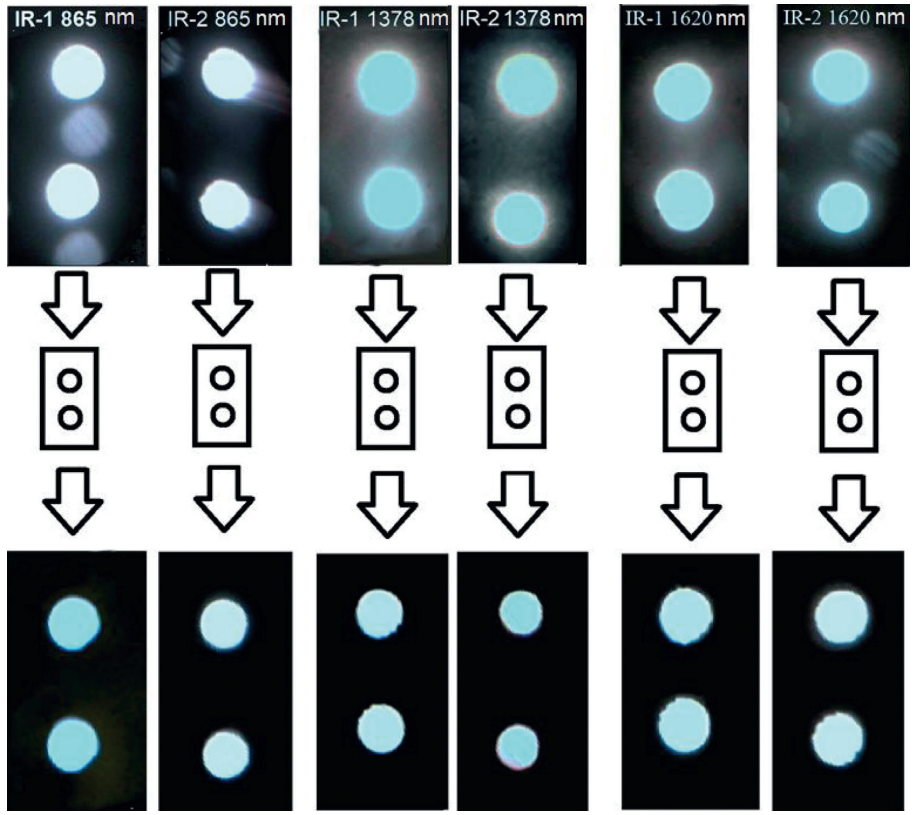

Figure 17: Image of field diaphragm in the focal planes of camera lenses for IR-1 and IR-2 units before and after input of blocking diaphragms.

calibration of ScanPol optical channels was successfully developed and tested using a numerical experiment based on the mentioned model, given the fixed values of the imperfections of its optical elements.

Furthermore, according to the calibration procedure described in [14], the experimental evaluation and calibration that are planned for each ScanPol spectral channel are provided.

5. Conclusion

This paper presents the results of the development of the representational model of the polarization state analyzer of the scanning polarimeter ScanPol for the Aerosol-UA space project designed to investigate the microphysical characteristics of an aerosol in the atmosphere.

The main characteristics of the optical system are given. An experimental sample of the polarization state analyzer ScanPol was designed, implemented, and assembled. The divergence of the optical axes of the input telescopic systems of the VIS-1, VIS-2, IR-1, and IR-2 units is determined experimentally. The maximum value is less than 1.5 arcmin.

This paper theoretically substantiates the minimum achievable error in determining the degree and azimuth of the polarization of the ScanPol incoming light with the given accuracy of determining the orientation of the Wollaston prisms axes.

The analysis was performed for optical ghosts that occur in the optical system and are formed in the focal plane of the camera lens. The position of the parasitic images is determined, and additional apertures are introduced to block them.

Data Availability

The data used to support the findings of this study are available from the corresponding author upon request.

Conflicts of Interest

The authors declare that there are no conflicts of interest regarding the publication of this paper.

Acknowledgments

This work was supported by the NAS of Ukraine under Target Comprehensive Program for Space Research for 2018–2022.

References

[1] P. F. Levelt, G. H. J. van den Oord, M. R. Dobber et al., "The ozone monitoring instrument," *IEEE Transactions on Geoscience and Remote Sensing*, vol. 44, no. 5, pp. 1093–1101, 2006.

[2] R. McPeters, M. Kroon, G. Labow et al., "Validation of the aura ozone monitoring instrument total column ozone product," *Journal of Geophysical Research*, vol. 113, no. D15, p. S14, 2008.
[3] Y. Shi, J. Zhang, J. S. Reid, B. Holben, E. J. Hyer, and C. Curtis, "An analysis of the collection 5 MODIS over-ocean aerosol optical depth product for its implication in aerosol assimilation," *Atmospheric Chemistry and Physics*, vol. 11, no. 2, pp. 557–565, 2011.
[4] D. J. Diner, S. W. Boland, M. Brauer et al., "Advances in multiangle satellite remote sensing of speciated airborne particulate matter and association with adverse health effects: from MISR to MAIA," *Journal of Applied Remote Sensing*, vol. 12, no. 4, Article ID 042603, 1 page, 2018.
[5] O. P. Hasekamp, G. Fu, S. P. Rusli et al., "Aerosol measurements by SPEXone on the NASA PACE mission: expected retrieval capabilities," *Journal of Quantitative Spectroscopy and Radiative Transfer*, vol. 227, pp. 170–184, 2019.
[6] Z. Li, W. Hou, J. Hong et al., "Directional Polarimetric Camera (DPC): monitoring aerosol spectral optical properties over land from satellite observation," *Journal of Quantitative Spectroscopy and Radiative Transfer*, vol. 218, pp. 21–37, 2018.
[7] G. Milinevsky, Y. Yatskiv, O. Degtyaryov et al., "New satellite project Aerosol-UA: remote sensing of aerosols in the terrestrial atmosphere," *Acta Astronautica*, vol. 123, pp. 292–300, 2016.
[8] M. I. Mishchenko, B. Cairns, G. Kopp et al., "Accurate monitoring of terrestrial aerosols and total solar irradiance: introducing the Glory mission," *Bulletin of the American Meteorological Society*, vol. 88, no. 5, pp. 677–692, 2007.
[9] O. P. Hasekamp and J. Landgraf, "Retrieval of aerosol properties over land surfaces: capabilities of multiple-viewing-angle intensity and polarization measurements," *Applied Optics*, vol. 46, no. 16, pp. 3332–3344, 2007.
[10] O. P. Hasekamp, "Capability of multi-viewing-angle photopolarimetric measurements for the simultaneous retrieval of aerosol and cloud properties," *Atmospheric Measurement Techniques*, vol. 3, no. 4, pp. 839–851, 2010.
[11] A. Russell, *Chipman, Wai Sze Tiffany Lam, Garam Young Polarized Light and Optical Systems*, CRC Press, Boca Raton, FL, USA, 2018.
[12] J. E. Hansen, "Circular polarization of sunlight reflected by clouds," *Journal of Atmospheric. Science*, vol. 28, no. 8, pp. 1515-1516, 1971.
[13] O. Dubovik, Z. Li, M. I. Mishchenko et al., "Polarimetric remote sensing of atmospheric aerosols: instruments, methodologies, results, and perspectives," *Journal of Quantitative Spectroscopy and Radiative Transfer*, vol. 224, pp. 474–511, 2019.
[14] G. Milinevsky, Y. Oberemok, I. Syniavskyi et al., "Calibration model of polarimeters on board the Aerosol-UA space mission," *Journal of Quantitative Spectroscopy & Radiative Transfer*, vol. 229, pp. 92–105, 2019.
[15] https://atmos.eoc.dlr.de/projects/scops/sciamachy_book/.
[16] B. Cairns and I. Geogdzhayev, *Aerosol Polarimetry Sensor Calibration, Glory Project, Goddard Space Flight Center, Greenbelt, Maryland --GSFC 421.7-70-03, Aerosol Polarimetry Sensor Algorithm Theoretic Basis Document*, 2010, http://glory.giss.nasa.gov/aps/docs/APS_ATBD_CALIBRATE_CCB.pdf.
[17] B. Cairns, E. E. Russell, L. D. Travis, D. Larry, and Travis, "Research Scanning Polarimeter: calibration and ground-based measurements," *Polarization: Measurement, Analysis, and Remote Sensing II*, vol. 3754, 1999.
[18] P. Goloub, B. Toubbe, M. Herman et al., "In-flight polarization calibration of POLDER," *Advanced and Next-Generation Satellites II, Proceedings of the SPIE*, vol. 2957, no. 24, 1997.
[19] W. Feng and L. Chen, "The impact of the orientation angles uncertainty of instrument polarizers on polarization measurement accuracy," *Optik*, vol. 121, no. 24, pp. 2276–2279, 2010.